River Flow 2010 - Dittrich, Koll, Aberle & Geisenhainer (eds) - © 2010 Bundesanstalt für Wasserbau ISBN 978-3-939230-00-7

Characteristics of the recirculation cell pattern in a lateral cavity

N. Riviere, M. Garcia, E. Mignot, G. Travin
Laboratoire de Mécanique des Fluides et d'Acoustique, Université de Lyon, France

ABSTRACT: The experimental work presented herein aims at studying the interaction between an open channel main stream and a rectangular lateral cavity in shallow water conditions. The main measurements concern the 2D recirculation pattern observed in the cavity and in particular the number and size of the 2D contra-rotating cells as a function of the main flow characteristics and the cavity dimensions. The innovative aspect of the experimental set-up used herein is that the length of the cavity (in the direction perpendicular to the main flow axis) can vary up to seven times the channel width. Surface tracers are inserted in the cavity, the cavity is placed in controlled light conditions and photos of the free surface are obtained where the recirculation pattern appears clearly. When increasing the cavity length, up to four recirculation cells are observed, with decreasing dimension and decreasing rotation velocity. The dimensional analysis reveals that the dimensionless length of each recirculation cell in the cavity is a function of 5 parameters: the dimensionless water depth, the Froude and Reynolds numbers of the main flow, the aspect ratio of the cavity and the bed friction number of the cavity. Four series of flow configurations are considered for four Froude number values. The dimensionless water depth affects both the size and the possible number of recirculation cells that form. Due to experimental limitations, it is difficult to sort the influence of the bed friction number, but its study seems to indicate that the Froude number has no noticeable influence.

Keywords: Cavity, Recirculation cell, Image analysis

1 INTRODUCTION

Lateral cavities are encountered in various open channel flow hydrodynamics situations. Oxbows, cut-off meanders form typical natural cavities connected to rivers. Harbors connected to a river or sea streams, groyne fields in rivers are typical artificial cavities. In the literature, side cavities are studied through two main physical phenomena. First one is the formation of vortices of vertical axis: the cavity is occupied by one or several recirculation cells. Second one is the appearance of free-surface oscillations.

At the connection between the main stream with uniform velocity and the cavity at rest, a large velocity gradient forms. This velocity gradient leads to a horizontal mixing layer which extends from the upstream corner to the downstream corner of the junction. This mixing layer transfers mass and momentum from the main flow to the cavity, and influences the number and the nature of the recirculation cells (2D or 3D). It is thus of primary importance for cavity performance, exchange of nutrients and gases influencing the ecological equilibrium of oxbows, or exchange of fine sediments influencing the geo-morphological efficiency of groyne fields. Moreover, the coherent vortex shed from the upstream corner to the downstream corner of the junction induce the excitation of the cavity resulting in large standing waves: this is the so-called "seiche" phenomenon.

Contributions concerning side cavities mix measured (based on PIV measurements and detailed below) and numerical approaches (Kimura and Hosoda, 1997; Nezu *et al.,* 2002 ; Mizumura and Yamasaka, 2002). Kodotani *et al.* (2008) measured simultaneously the velocity field at the surface and surface level oscillations to correlate seiching and streamwise velocity in the main stream. Literature on groyne fields focuses more on the number of recirculation cells and the exchanges between the mainstream and the cavity.

Such experiments are proposed by Langendoen *et al.* (1994), Uijtewaal *et al.* (2001), Weitbrecht *et al.* (2008). They show that, compared to a single cavity, the groyne fields are characterized by the interaction between the successive cavities. Recent numerical contributions are the ones of Hinterberger *et al.* (2007) and McCoy *et al.* (2008), the latter emphasizing on the three-dimensionality of the flow in the cavity, with a compound channel.

When focusing on the recirculation cell patterns that develop in the cavity, the main parameter emerging from literature is the aspect ratio L/b of the cavity. Here, we define L as the cavity length (along the crosswise direction, perpendicularly to the main stream direction) and b as its width. For $L/b \approx 1$, a single recirculation cell occupies the whole cavity; smaller values of L/b correspond to two cells along the transverse direction. Weitbrecht *et al.* (2008)'s experiments, with L/b reaching 3.3, show the appearance of a second recirculation in the crosswise direction.

Present contribution takes advantage of an experimental facility that allows aspect ratio reaching more than 6.5, with other dimensions comparable to previous experiments (Table 1). This permits to observe original flow patterns – with as much as four cells - that are analyzed in the sequel.

After describing the experimental set-up, these new flow patterns are presented briefly. Then, the dimensional analysis is performed before exposing the experimental results. Finally, results are discussed before concluding the paper.

2 EXPERIMENTAL SET-UP

The experiments are performed in the channel intersection facility at the Laboratoire de Mécanique des Fluides et d'Acoustique at the Université de Lyon. The facility consists of three glass channels of rectangular shape sections, 0.3m wide and 2m long, which intersect at 90° and with slopes that can be varied independently (see Fig. 1). For the supercritical configurations, the slopes of the upstream and downstream branches of the main channel are fixed to s = 7.4% while for the subcritical configurations, they remain horizontal. Moreover, the junction and the side channel remain horizontal for all experiments. The upstream branch of the main channel provides the inlet flow, the downstream branch of this channel acts as outlet channels and the side channel is closed with no inflow or outflow. A honeycomb at the inlet of the upstream branch serves to stabilize and straighten the inlet flow. For the supercritical configurations, the flow depth is imposed using a vertical sluice gate. For the subcritical configurations, surface waves are eliminated by means of a sheet of polyurethane floating on the free surface and a sharp crested weir is used to fix the water depth at the outlet section of the downstream branch. The inlet discharge Q varies in the range 0.53-7 l/s. Corresponding water depth based Reynolds number range is 7200-92000. The length of cavity (noted L herein) is easily modified by fixing an end wall in the side channel at a given distance from the junction. This wall is made by a sheet of polyurethane with a flat gasket ensuring its tightness. A glass plate is bonded on the wall to have the same wave reflection capacity as the one of the channel walls. On the other hand, the width of the cavity (noted b) remains constant, equal to the width of the main channel ($b=30$ *cm*). The aspect ratio of the cavity (L/b) can vary from 0 up to 6.6 as L varies from 0 to 2m.The measured flow parameters are i) the flow rate in the main channel (noted Q herein), measured using an electromagnetic flowmeter (Promag 50 from Endress Hauser; accuracy of ±0.05 L/s) and ii) the water depth in the junction (noted h), measured using a point gauge with an accuracy of ±0.15 mm. A camera is fixed above the cavity, a horizontal sheet of white light is created at the free

Table 1. Range of parameters in previous works

	b(cm)	*L/b*	*h(cm)*	*Fr*	*Re*
Kimura & Hosoda, 1997	15-22.5	0.7-1	1-2	0.8	2800-8000
Mizumura & Yamasaka, 2001	8-16	0.5-1	4.5	0.2-0.8	6000-24000
Uijttewaal *et al.*, 2001	107-225	0.3-0.7	10	0.3	35000
Nezu & Onitsuka, 2002	20	0.2	4	0.5	12300
Booij, 2004	100-300	1	10	0.2	50000
Uijttewaal, 2005	450	0.4	25	0.2	87500
LeCoz *et al.*, 2006	10	0.5	10.7	0.4	38950
Hinterberger *et al.,* 2007	125	0.4	4.7	0.2	7440
Weitbrecht *et al.*, 2008	15-145	0.3-3.3	46	0.1	73600
McCoy *et al.,* 2008	107.5	0.7	4	0.6	14000
Kadotani *et al.*, 2008	25-35	0.2-0.3	4	0.6-0.8	-
Present work	30	0-6.6	0.58-7	0.2-4.8	6200-77500

surface level in the cavity and the whole experimental set-up is positioned below an opaque tent. Tracers (grass seeds) floating at the free surface are finally introduced in the cavity and photographs of the free surface are taken with controlled time exposure (from a few seconds to about two minutes).

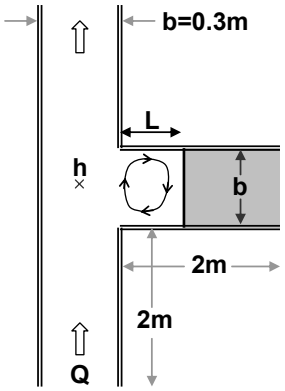

Figure 1. Scheme of the experimental set-up.

3 QUALITATIVE DESCRIPTION

Due to flow entrainment, a first clockwise recirculation cell is observed in the cavity in the region near the junction. However, according to the geometric and flow parameters, additional cells can appear with varying organization (location and size). For instance, when increasing the cavity length value L, the number of cells increases:

* For a small cavity, two recirculation cells aligned along the transverse direction of the cavity are observed. The main cell (on top of the photo in Fig. 2) is clockwise and the secondary cell on the upstream region but shifted away from the main stream is anti-clockwise.

* For a slightly larger cavity length, a single clockwise recirculation takes place, which occupies the whole cavity area (see Fig. 3).

* When increasing the cavity length, a second recirculation cell (anti-clockwise) is observed. Both cells occupy the whole cavity width but the second cell is confined at the extremity of the cavity.

* For larger cavity lengths, a third and even a fourth cell are observed (see Fig. 4).

* For a very large cavity length, an additional area with no vorticity is observed at the extremity of the cavity (see Fig. 5). Nevertheless, this region is not at rest as a very slow surface motion directed toward the main stream is observed (the exposure time is equal to 196 seconds for this photo).

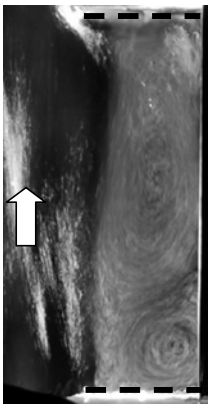

Figure 2. Recirculation pattern with two cells along the transverse direction of the cavity.

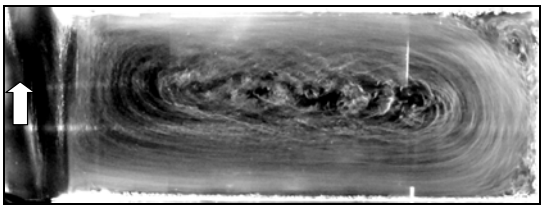

Figure 3. Recirculation pattern with a single cell.

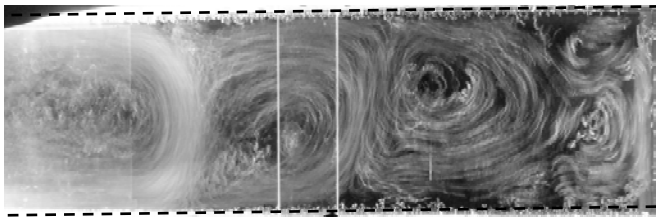

Figure 4. Recirculation pattern with four cells.

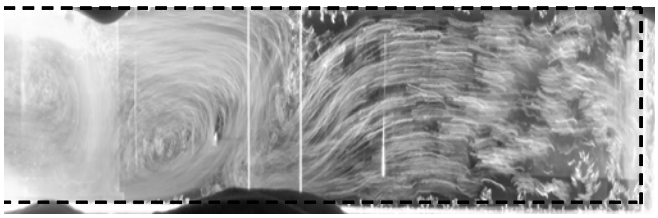

Figure 5. Two recirculations pattern with an additional area with no vorticity.

4 DIMENSIONAL ANALYSIS

The geometrical parameters and flow parameters that influence the number of recirculation cells in the cavity and their size l_i (i=1,2,3,4) are: the bulk velocity U and water depth h in the main channel, the cavity length L, the main channel and cavity width b, the Darcy wall friction coefficient λ, the kinematic viscosity ν and density ρ of the fluid, the gravity g. Based on these 8 parameters, it is possible to write:

$$\frac{l_i}{b} = f\left(\frac{L}{b}, \frac{h}{b}, F_r, R_e, S\right) \quad (1)$$

with $F_r=U/(gh)^{0.5}$ the Froude number, $Re=4Uh/\nu$ the Reynolds number of the main flow and $S=\lambda L/8h$ a bed friction number (Babarutsi *et al.,*

1989) based on the cavity length and the Darcy friction coefficient. In a first approach, we will neglect the influence of R_e. Eq. 1 thus becomes:

$$\frac{l_i}{b} = f\left(\frac{L}{b}, \frac{h}{b}, F_r, S\right) \quad (2)$$

The meaning of *L/b* (cavity geometrical characteristics) and *Fr* (main stream dynamics) is obvious. It does not hold for *h/b* and *S*. *h/b*, dimensionless water depth, is expected to account for the three-dimensionality of the flow in the cavity (evolution of the velocity direction from the bottom to the free surface). *S* accounts for the vertical confinement effect. This effect governs the inability (or ability) of horizontal large scale vortices to develop in the crosswise direction (along L), because of the vertical shear between the bed and the free-surface (Babarutsi *et al.*, 1989; Uijttewaal and Booij, 2000; Chu *et al.*, 2004).

The final objective will be to investigate the influence of each parameter of Eq. 2 without altering the value of the other ones. However, altering one among the three following parameters *S*, *L/b* or *h/b* without altering the two others requires modifying the friction coefficient λ in the cavity. This will be performed in future tests by changing the wall roughness in the cavity but was not performed here. Experimentally, modifying *L* is performed by moving the end wall in the cavity. For the supercritical conditions, modifying *h* or *Fr* is performed by changing i) the upstream sluice gate opening, ii) the channel slope and iii) the main flow discharge. For the subcritical conditions (horizontal channels), modifying *h* or *Fr* is performed by changing i) the downstream weir height, and ii) the main stream discharge.

5 RESULTS

5.1 *Influence of dimensionless cavity length L/b*

In this section, we describe the flow pattern that is observed as the cavity length *L* is altered while keeping the other parameters constant. As explained above, as *L* increases, a single cell is first observed and occupies the whole cavity length (l_1=*L*), then 2, 3 and in some cases 4 cells are observed with $\Sigma\, l_i = L$. Finally, a dead zone may be observed for very large cavity lengths.

For a selected subcritical configuration, Fig. 6 confirms that until T_{12} (the 1 to 2 cell transition), a single cell is observed, it occupies the whole cavity length. Then as *L* increases, the second cell appears and occupies more that the additional length: the length of the first cell l_1 decreases suddenly. Then as *L* increases again, the size of the second cell l_2 increases as l_1 remains constant for all values of *L*. At transition T_{23} the third cell appears and l_2 decreases suddenly; then l_2 remains constant for larger values of *L*. Finally, at transition T_{34} the fourth cell appears and again l_3 decreases suddenly.

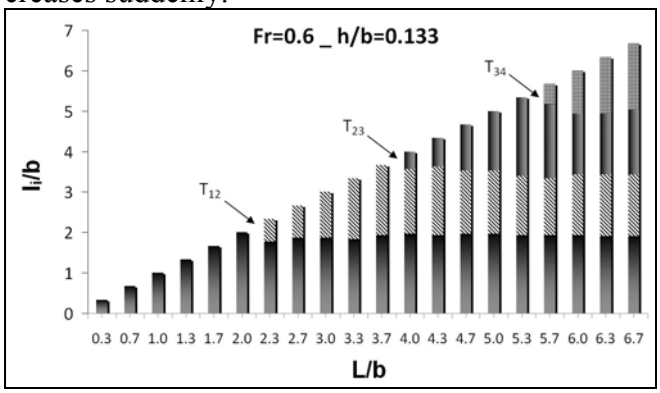

Figure 6. Number and length of the four observed recirculation cells with varying cavity length for *Fr=0.6* and *h/b=0.133*.

Fig. 7 presents the same data as Fig. 6 and permits to confirm that as *L* increases between two consecutive transitions, the furthest cell length l_i increases, following exactly the total length increase *L*.

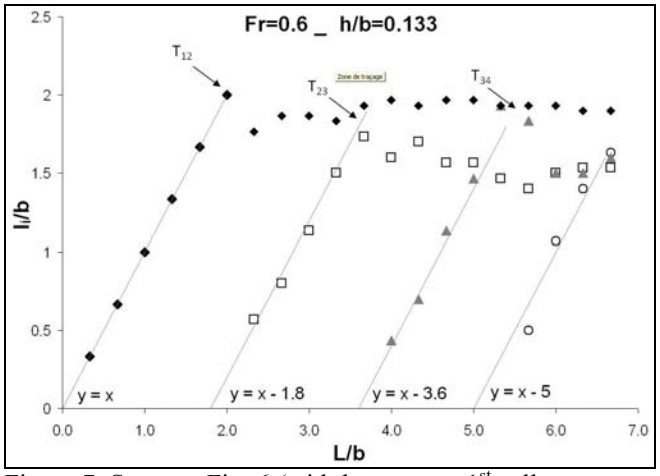

Figure 7. Same as Fig. 6 (with lozenges = 1st cell, squares = 2nd cell, triangles = 3rd cell and circles = 4th cell).

A similar behavior is observed for supercritical inflow configurations (not shown here). The only difference between the various configurations lies in the dimensionless cavity length value *L/b* at which the transitions T_{12}, T_{23} and T_{34} occur. This will be investigated in the following section.

5.2 *Influence of dimensionless water depth h/b*

For more convenient presentation, each transition will be presented one after the other in this section. For all flow configurations detailed in Table 2, the following figures will show the corresponding *L/b* and *h/b* parameters obtained at the three first transitions.

Fig. 8 shows that for the three subcritical main stream configurations, the dimensionless cavity length L/b at which the first transition T_{12} occurs does not depend on the main stream Froude number Fr nor on the dimensionless water depth h/b. For all subcritical data, the second cell appears for $L = 2.33b$ as was already seen on Fig. 6 and 7. Oppositely, for the supercritical available configuration, it appears that as the water depth h/b increases, the first transition occurs for increasing dimensionless cavity length L/b. Moreover, it appears that for both largest water depths, the first transition occurs at similar cavity lengths as for the subcritical conditions. It would be interesting to verify wether the first transition would appear for lower cavity length in case of lower water depth conditions in subcritical regime. More experiments are required before concluding.

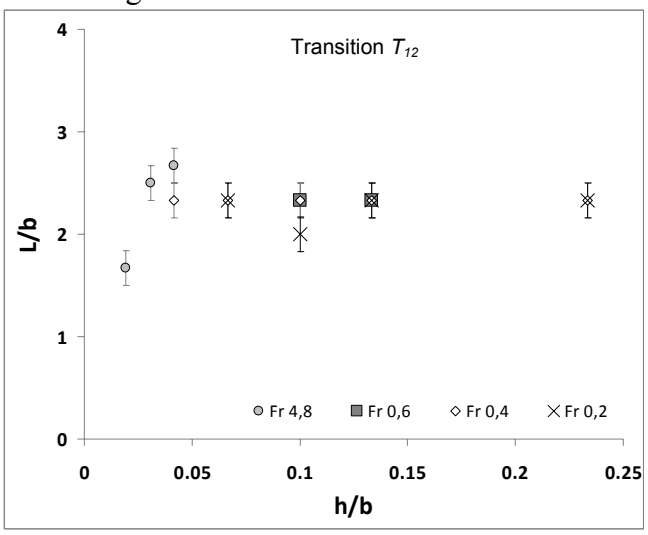

Figure 8. Flow conditions for which the transition T_{12} was observed for all flow configurations

Fig. 9 confirms that the second transition T_{23} occurs obviously for larger dimensionless cavity lengths L/b than for the first transition and that this L/b value is quite constant ($L/b=4$) for all Fr and h/b values in subcritical conditions except for the largest dimensionless water depth values.

As emphasized in section 4, h/b accounts for the three-dimensionality of the flow in the cavity. Indeed, Booij (2004) indicates for decreasing cavity shallowness (or increasing h/b), the secondary current development is enhanced. These secondary currents, caused by centrifugal forces in the cavity, are responsible for the entrainment of water in the centre of the cavity by the peripheral circulation. Booij (2004) proposes that the whole cavity is entrained, as soon as $h/b>0.1$. This is consistent with our results where, on both figures 8 and 9, where the dimensionless length L/b corresponding to the transitions no more depends on h/b when $h/b>0.1$.

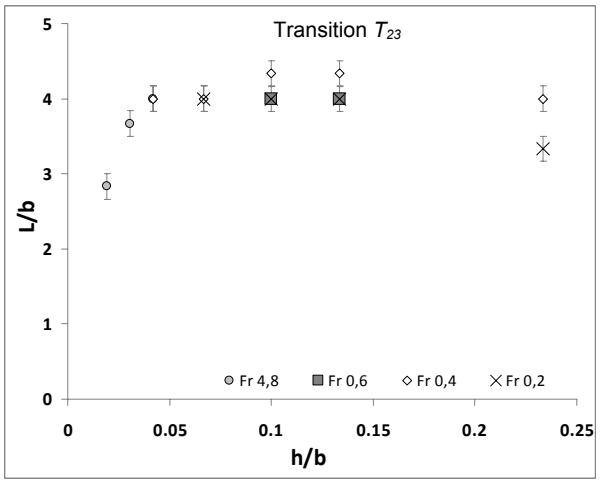

Figure 9. Flow conditions for which the transition T_{23} was observed for all flow configurations

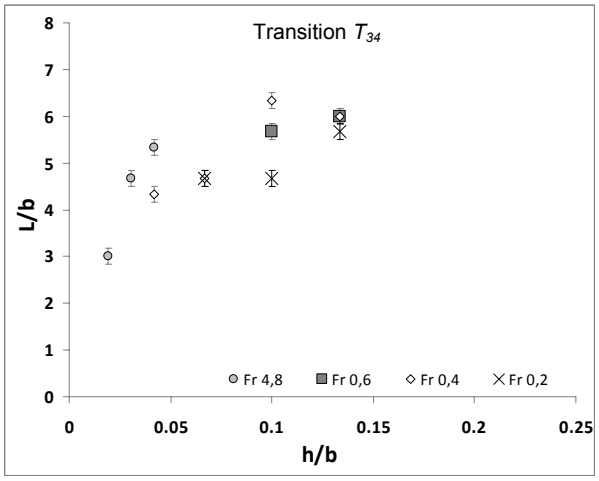

Figure 10. Flow conditions for which the transition T_{34} was observed for all flow configurations

As expected, the third transition T_{34} shown on Fig. 10 occurs for larger cavity length than both previous transitions. Though the data are more scattered than for the two previous transitions, some trends can be underlined. First, for $h/b<0.1$, L/b seems again to increase with h/b while no Froude number tendency is observed. Second, it is worth seeing that for the highest h/b values ($h/b=0.23$), no fourth recirculation exist. Only three cells are observed, the rest of the cavity space being occupied by a dead zone as the one shown on Fig. 5. This photograph shows velocity directed towards the main stream on the whole dead zone, which must be balanced by an inward velocity near the bed, confirming the presence of secondary currents. This was observed by McCoy *et al.* (2008) in their numerical study of the exchanges between the stream and the cavity.

5.3 *Influence of the bed friction number S*

As mentioned in section 4, S is expected to have a different meaning from h/b as it accounts for the

vertical confinement effect, i.e. the ability of horizontal large scale vortices to develop in the transverse direction (Babarutsi *et al.*, 1989). The influence of S on the first transition is sketched on Fig.11 The supercritical and subcritical data follow the same evolution: as S increases, the dimensionless cavity length L/b at which the transitions occur decreases, especially for high S values. Nevertheless, Fig.11 is quite similar to Fig.9 with a reverse abscissa axis. Indeed, keeping the same wall roughness in our limited range of Reynolds number, λ experiments little variations and the influence of S follows more or less the one of h/b. Additional experiments with an increased wall roughness are required to sort the influence of these two parameters.

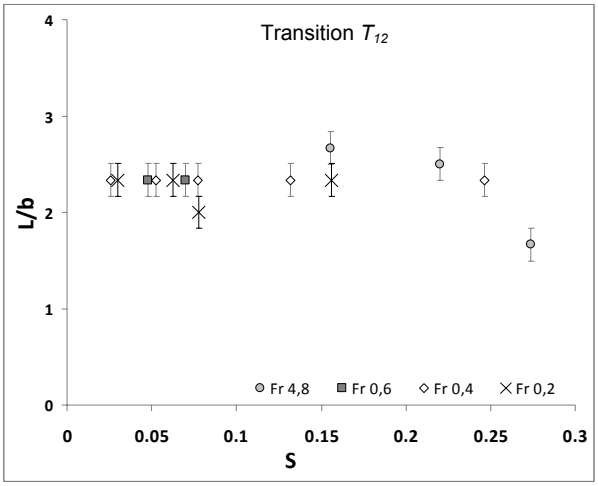

Figure 11. Flow conditions for which the first transition was observed as a function of the cavity friction number.

6 DISCUSSION

The evaluation of energy dissipation between the various cells appears to be necessary in order to understand why a given number of cell is the most stable pattern for a given flow configuration.

Fig. 12 shows photographs of a four-cell pattern obtained using four different time-exposures. The first cell is clearly visible with the lowest time-exposure while the further cells need a larger time-exposure. This statement reveals that the rotation velocity is low in the last cells and is maximum in the first cell.

The energy passed from the main channel to the recirculation cells is transferred through the mixing layer at the frontier between the main stream and the first cell. This energy is then dissipated within the cavity through shear stresses at all velocity gradient regions, that is: (1) vertical and horizontal gradient of velocity due to the no slip condition at the bottom and the side walls of the cavity and (2) horizontal gradient of velocity between two consecutive contra-rotating cells.

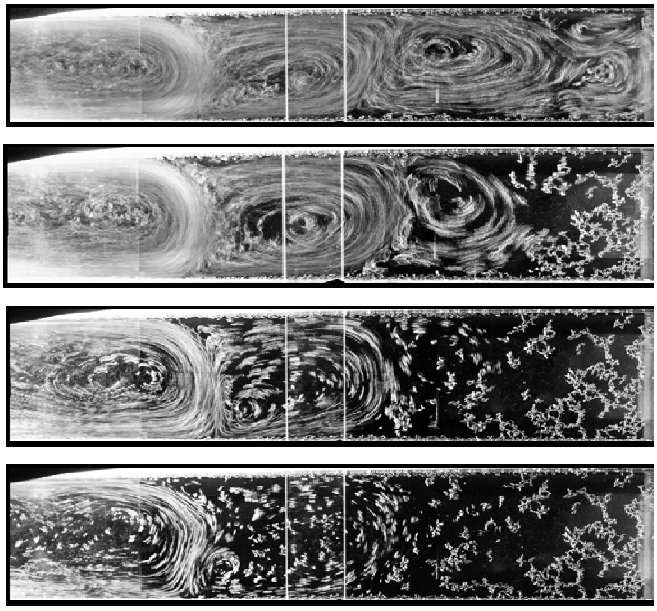
Figure 12. Flow configuration with four recirculation cells observed with four exposure times (from top to bottom: 30s, 20s, 2s, 1.2s).

It should be noted that increasing the cavity length L affects the rotation velocity of the first cell and thus the velocity gradient between the main channel and this cell. It may thus modify the total quantity of energy passing from the main channel to the cavity. In such case, it becomes impossible to compare the energy dissipated by a single cell and two or more cells when increasing L/b. More, the effective part of the cavity which is in rotation seems to vary under the influence of the secondary currents.

Hence, evaluating the energy dissipation requires completing the present experiments by measuring velocity fields. They would give access to velocity gradients and energy or momentum transfers from the mainstream to the first cell, and then from one cell to another.

Table 2. Measured flow configurations

Fr	Q (l/s)	h (mm)
4.8*	2 - 4 - 6.3	5.8 - 9.2 - 12.5
0.6	2.9 - 4.5	30 - 40
0.4	0.53 - 1.06 - 1.95 - 3 - 7	12.5 - 20 - 30 - 40 - 70
0.2	0.53 - 1 - 1.5 - 3.5	20 - 30 - 40 - 70

* The channel slope s=7.4% while for other cases s=0.

7 CONCLUSIONS

Experiments were performed on recirculating flows in side cavities connected to a free stream. Thanks to the experimental facility used here, it was possible to obtain up to four consecutive contra-rotating recirculating cells in one cavity.

The dimensional analysis showed that the number of cells and their sizes depend on three dimensionless parameters, apart from the Reynolds number: the cavity aspect ratio L/b, the di-

mensionless main stream depth *h/b* and the main stream Froude number *Fr*. It appears from the present data that there is practically no effect of the three parameters on the number of cells and their lengths. At this time, experimental limitations have prevented us to make vary each parameter independently from the two others. Thus, there are some works in prospects to emit more definite conclusions.

Indeed, sorting the influences of *h/b* and *Fr* will be possible only by producing very shallow flows in subcritical regime. This is forbidden by the downstream conditions of the present facility. Moreover, sorting the influence of *h/b* and *S* will be enabled by using different wall roughness, in order to vary the friction coefficient λ for constant *h/b*. Finally, velocity field measurements will be performed. They are indeed required in order to evaluate the evolution of the velocity inside the recirculation cells when varying the various parameters and understand the energy transfers from one cell to another and from the free-surface to the bed region.

8 REFERENCES

Babarutsi, S., Ganoulis, J., Chu, V.H.. 1989. "Experimental investigation of shallow recirculating flows". *Journal of Hydraulic Engineering*, Vol.115, No.7, 906-924.

Booij R., 2004. Shallowness and longitudinal dispersion in rivers. 1175-1182. Riverflow 2004. Napoli, Italy, june 23-25.

Chu, V.H., Fang, L., Altai, W. 2004. Friction and confinement effects on a shallow recirculating flow, Journal of Environmental and Engineering. Science, 3(5), 463-475.

Hinterberger C., Fröhlich J., Rodi W. 2007. Three-dimensional and Depth-averaged Large-Eddy simulations of some shallow water flows. Journal of Hydraulic Engineering, 133(8), 857-872.

Kadotani K., Fujita I., Matsubara T., Tsubaki R. 2008. Analysis of water surface oscillation at open channel side cavity by image analysis and large eddy simulation. ICHE conference, Nagoya, Japan, sept. 9-12.

Kimura I., Hosoda T. 1997. Fundamental properties of flows in open channels with dead zone. Journal of Hydraulic Engineering, 123(2), 98-107.

Langendoen E.J., Kranenburg C., Booij R. 1994. Flow patterns and exchange of matter in tidal harbours. Journal of Hydraulic Research, 32(2), 259-270.

Le Coz, J., W. Brevis, Y. Niño, A. Paquier et N. Rivière. 2006. Open-channel side-cavities: a comparison of field and flume experiments. River Flow 2006, vol 1, 145-152, Lisbonne, Portugal, sept. 6-8.

McCoy A., Constantinescu G. and Weber L. J. 2008. Numerical Investigation of Flow Hydrodynamics in a Channel with a Series of Groynes. Journal of Hydraulic Engineering, 134(2), 157-172.

Mizumura K., Yamasaka M. 2002. Flow in open channel embayments, Journal of Hydraulic Engineering, 128(12), 1098-1101.

Nezu I. et Onitsuka K., 2002. PIV Measurements of Side-Cavity Open-Channel Flows – Wando Model in Rivers. , Journal of Visualization, 5(1), 77-84.

Uijttewaal, W., Booij, R. 2000. Effects of shallowness on the development of free-surface mixing layers. *Physics of Fluids*, Vol.12, No.2, 392-402.

Uijtewaal W., Lehmann D., van Mazijk A. 2001. Exchange processes between a river and its groyne fields : model experiments. Journal of Hydraulic Engineering, 127(11), 928-936.

Uijtewaal W. 2005. Effects of groyne layout on the flow in groyne fields : Laboratory experiments. Journal of Hydraulic Engineering, 131(9), 782-791.

Weitbrecht V., Socolofsky S. A. et Jirka G. H. 2008. Experiments on Mass Exchange between Groin Fields and Main Stream Rivers, Journal of Hydraulic Engineering, 134(2), 173-183.